

Orbital localization and the role of the Fe and As $4p$ orbitals in BaFe_2As_2 probed by XANES

A. G. de Figueiredo¹, M. R. Cantarino¹, W. R. da Silva Neto^{1,2}, K. R. Pakuszewski³, R. Grossi³, D. S. Christovam^{3*}, J. C. Souza³, M. M. Piva^{3*}, G. S. Freitas³, P. G. Pagliuso³, C. Adriano³, F. A. Garcia¹

¹*Instituto de Física, Universidade de São Paulo, São Paulo-SP, 05508-090, Brazil*

²*Instituto de Química, Universidade de São Paulo, São Paulo-SP, 05508-090, Brazil and*

³*Inst Fis Gleb Wataghin, Universidade Estadual de Campinas, Campinas-SP, 13083-859, Brazil**

The polarization dependence of the near edge x-ray absorption spectroscopy (XANES) is an element specific probe to the real-space distribution of the density of unoccupied states in solid-state materials. In this paper, we present Fe and As K -edge experiments of $\text{Ba}(\text{Fe}_{1-x}\text{M}_x)_2\text{As}_2$ ($M = \text{Mn}, \text{Co}$ and $x = 0.0$ and 0.08). The experiments reveal a strong polarization dependence of the probed XANES spectra, which concerns mainly an increase of the intensity of electronic transitions when the beam polarization is set out of the sample's ab crystallographic plane. The results show that states with p_z -orbital character dominate the density of unoccupied states close to the Fermi level. Partial substitution of Fe by Co is shown to decrease the intensity anisotropy, suggesting that Co promotes electronic transfer preferentially to states with p_z -orbital character. On the other hand, Mn substitution causes the increase of the spectra p_z -orbital anisotropy, which is proposed to take place by means of an enhanced local Fe $3d4p$ mixing, unveiling the role of Fe $4p$ states in the localization of the Fe $3d$ orbitals. Moreover, by comparing our results to previous experiments, we identify the relative mixing between Fe and the pnictide $4p_{x,y,z}$ orbitals as a clear divide between the electronic properties of iron arsenides and selenides. Our conclusions are supported by multiple-scattering theory calculations of the XANES spectra and by quantum chemistry calculations of Fe coordination electronic structure.

I. INTRODUCTION

Doping an electronic correlated phase often results in rich phase diagrams containing regions dominated by strong electronic correlations and other regions wherein Fermi liquid behavior is observed. The relatively recently introduced Fe pnictide (FePns) materials [1] denote a large family of high-temperature unconventional superconducting materials that seems to lie on the border between weak and strong electronic correlations [2]. Indeed, the description of the relevant electronic degrees of freedom in terms of either localized or itinerant states underlines a major conceptual divide in this field [3–6].

The 122 parent compound BaFe_2As_2 is a particularly well explored FePn material. Phases derived from the partial substitution of Fe by Co, $\text{Ba}(\text{Fe}_{1-x}\text{Co}_x)_2\text{As}_2$, is a much debated subject mainly because it leads to a robust and clean superconducting (SC) ground state [2, 7]. In the case of $\text{Ba}(\text{Fe}_{1-x}\text{Mn}_x)_2\text{As}_2$, however, no SC phase is observed [8]. In principle, partial substitution at the Fe site by Mn pushes the BaFe_2As_2 electronic properties to a Mott region, whereas partial substitution by Co tends to decrease its electronic correlations. Indeed, the endpoints of the $\text{Ba}(\text{Fe}_{1-x}\text{M}_x)_2\text{As}_2$ ($M = \text{Mn}$ or Co) materials, BaMn_2As_2 and BaCo_2As_2 , are characterized as an antiferromagnetic Mott insulator [9, 10] and a weakly correlated metal [11, 12], respectively, somehow corroborating the proposed substitutional trends.

The BaFe_2As_2 structure features FeAs layers well spaced by Ba^{2+} cations, where Fe is fourfold coordinated by As atoms arranged in a slightly distorted tetrahedral geometry. This structure breaks the degeneracy of the Fe derived $3d$

states close to the Fermi level, directly affecting the BaFe_2As_2 Fermi surface composition, making the Fe coordination an important parameter to understanding the 122 materials electronic properties [2]. In this work, we focus precisely on the electronic properties of the FeAs coordination complex, investigating the polarization and composition dependencies of the near edge (XANES) Fe and As K -edges X-ray absorption spectra of $\text{Ba}(\text{Fe}_{1-x}\text{M}_x)_2\text{As}_2$ ($M = \text{Mn}$ or Co , $x = 0.0$ and $x = 0.08$) single crystals.

Hard X-ray absorption spectroscopy (XAS) experiments could provide a handful of key information to the field of the FePns materials, including the role of transition metal substitution on their electronic [13–18] and structural properties [19–24], as well as the degree of electronic correlations [18, 25–27] in these systems. Here, we take advantage of the dipole selection rules dependence on the beam polarization that makes the XAS spectra strongly angular dependent. Focusing on the XANES region of the XAS spectra, we thus probe, in real space, the distribution of the density of unoccupied electronic states in our materials.

For all investigated materials, our results suggest that the density of unoccupied states at Fermi level has a predominant p_z orbital character, in agreement with the case of the iron arsenide SmFeAsO [28]. Co substitution is shown to populate preferentially the As $4p_z$ orbitals, characterizing a distinct charge transfer anisotropy. Mn substitution increases the spectra p_z orbital anisotropy suggesting the localization of the Fe $3d$ and A $s4p$ states, adding yet another piece of evidence that the BaFe_2As_2 material can be tuned to a correlated electronic phase [25], but this time not by doping. From our calculations and experiments, we conclude that the BaFe_2As_2 electronic structure displays a delicate interplay between the local Fe $3d4p$ mixing and the metal-to-ligand Fe $3d$ As $4p$ mixing. Our findings unveil the role of the Fe $4p$ states and allow one to make a clear distinction between the iron arsenides and the iron selenides, for which the unoccupied states were found to

* Current address: Max Planck Institute for Chemical Physics of Solids, Nöthnitzer Straße 40, 01187 Dresden, Germany

have a predominant Se $4p_{xy}$ character [29].

Our experiments are analyzed based on two complementary frameworks. We first present multiple scattering theory calculations (as implemented by the FEFF8.4 code [30, 31]), where we found relative agreement between our calculations and experiments for the Fe K -edge and As K -edge. Nevertheless, FEFF is not able to capture the angular dependence of the probed spectra. Then, we present multiconfigurational electronic structure calculations of the orbital states of a single FeAs₄ coordination complex, as implemented by ORCA 5.0 [32, 33].

II. MATERIAL AND METHODS

Ba(Fe_{1-x}M_x)₂As₂ ($M = \text{Mn or Co}$, $x = 0.0$ or 0.08) single crystals were synthesized by an In-flux technique as described in Ref. [34]. The Laue patterns of all samples were obtained to determine the relative orientation of the a and b crystallographic axis. A composition (x) vs. temperature (T) phase diagram of Mn and Co substituted samples is presented in Fig. 1(a) for context. Black squares and blue circles mark the data from Ref. [35] and red stars mark the data for our samples, as determined from resistivity measurements [34, 36, 37]. The investigated samples are indicated by black arrows.

The Fe K -edge and As K -edge hard X-ray absorption spectroscopy experiments were performed at the XDS beamline [38] of the Brazilian Synchrotron Light source (CNPEM-LNLS) at room temperature. Data was acquired by the partial Fe and As fluorescence. The samples were mounted in a Huber 6 + 2-circle diffractometer with the experimental geometry as explained in Fig. 1(b). The beam polarization direction is fixed and is aligned to one of the sample crystallographic axes, which will be hereafter called the a axis. XANES spectra were thus collected for rotations about the in plane a and b axis and the out of plane c axis which are, respectively, termed θ , ϕ and χ rotations (see Fig. 1(b)). For all rotations, we adopted an angular (α) interval of $0 < \alpha < 45^\circ$. All spectra were normalized in ATHENA [39].

FEFF calculations [31] were adopted to calculate the XANES spectra. The *ab initio* calculations were performed and converged for clusters of up to 282 atoms for the Fe K -edge and 144 atoms for the As K -edge. In both cases, the Hedin-Lundqvist [40] pseudopotential was adopted to account for the effect of the local exchange-correlation. Self-consistent calculations were performed for a cluster radius of 6.5 Å (Fe K -edge) and 8.0 Å (As K -edge). Quadrupolar transitions and spin orbit coupling effects were considered but no sizable effects were observed. Chemical substitution effects were simulated in the case of the As K -edge, by substituting one in ten Fe atoms by one Mn (Co) atom. The large self-consistent 8 Å radius was adopted to include all dopants in the self-consistent calculations.

Multiconfigurational electronic calculations of the electronic states of a FeAs₄ tetrahedral like molecule were implemented by ORCA 5.0 [32, 33]. Ionic charges were set as -3 for each arsenic ion and $+2$ for the metallic center, resulting in a $S = 2$ molecule, consistent with a high spin complex

within tetrahedral like coordination (D_{2d} symmetry). Atomic positions were obtained from the BaFe₂As₂ crystallographic data.

To capture the optimized configuration of the electronic states in this $3d$ metal complex, we apply the CAS-SCF method and electronic correlations were later taken into account by NEVPT-2 calculations. The relativistic adapted Karlsruhe valence triple-zeta with two sets of polarization functions were adopted as the basis set within the ZORA approximation [41]. We built a complete active space (CAS) consisting only of the five $3d$ orbitals and its six electrons - CAS(6,5) - in the D_{2d} symmetry, and the ligand Field Parameters were obtained at the end of the calculation. Virtual states, 5eV above the Fermi level, were calculated similarly but adopting a CAS(2,12) [42].

III. RESULTS AND DISCUSSION

In Figs.1 (c) and (d) we present representative normalized ($\mu(E)$) Fe and As K -edge spectra of BaFe₂As₂ along with their respective spectra derivatives. The Fe K -edge XANES spectrum presents five absorption features labeled by capital letters $A - E$. The features are positioned in the mid range between the maxima and minima of the spectrum derivative. Features $A - C$ are of electronic nature, whereas features D and E are predominantly due to scattering processes [13–15].

The A feature sits at about E_F , which is found to be $E_F \approx 7111.6$ eV. This feature is called the pre-edge and is understood to stem from a dipolar transition from the Fe $1s$ to Fe $3d$ As $4p$ hybrid bands. It comprises a series of energy levels located in a $1 - 2$ eV bandwidth about E_F and expresses the properties of the FeAs tetrahedral coordination complex. Feature B denote transitions to hybrid states (including Fe $4s$ and As $4p$ states) lying 3 eV above the Fe $3d$ As $4p$ states. Feature C , at about ≈ 7118.6 eV, is the main atomic transition of the Fe K -edge and stems from Fe $1s \rightarrow 4p$ transitions [43, 44].

The As K -edge XANES spectrum in Fig.1 (d) display two main features, which we called F and G . The former identify the main As $1s \rightarrow 4p$ atomic electronic transition which, due to the As coordination, also includes contributions from Fe $3d$ orbitals. The latter is mainly due to scattering processes and transitions to excited electronic states 5 eV above E_F . The F feature sits about $E_F \approx 11864.3$ eV.

In Fig.1 (e) – (g) we present the Fe K -edge spectra of BaFe₂As₂ for all investigated rotations. In its local coordinate frame, rotating the sample is equivalent to changing the incident beam polarization, which leads to new selection rules for the dipole transitions. A θ rotation is thus a control experiment, which does not change the beam polarization. Indeed, a direct inspection Fig.1(e) reveal that θ rotations do not change the spectra. A χ rotation probes orbitals with planar components (as the p_x and p_y p -orbitals) whereas ϕ rotations probe orbitals with z symmetry, as p_z orbitals.

The pre-edge intensities of the observed spectra clearly increase under ϕ rotations (Fig.1(f)) characterizing the spectra anisotropy. The inset in Fig.1(f) display the difference spectrum, obtained from making $\mu(E, \phi = 45^\circ) - \mu(E, \phi = 0^\circ)$. As

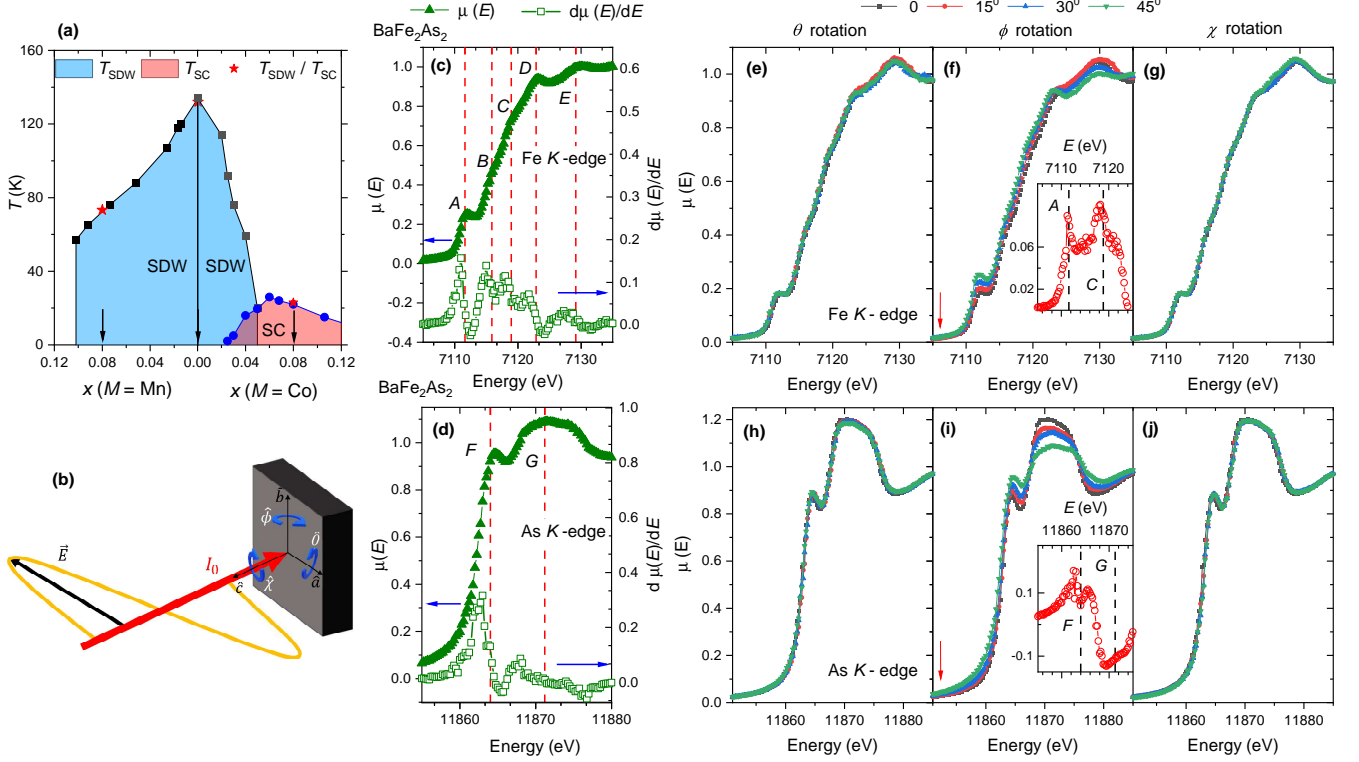


Figure 1. (a) Composition (x) vs. T phase diagram for the $\text{Ba}(\text{Fe}_{1-x}\text{Mn}_x)_2\text{As}_2$ and $\text{Ba}(\text{Fe}_{1-x}\text{Co}_x)_2\text{As}_2$ transition metal substituted iron arsenides (black squares are data from Ref. [35]). (b) Schematic representation of the experimental geometry, defining the rotation angles ϕ , θ and χ as rotations around the a , b and c axis, respectively. (c) Representative BaFe_2As_2 Fe K -edge normalized XANES spectrum ($\mu(E)$, left axis, full symbols) and its derivative ($d\mu(E)/dE$, right axis, open symbols). Capital letters A-E mark the transitions and the dashed lines associate the features in the spectrum derivative to the spectrum. (d) The respective As K -edge data of BaFe_2As_2 , with capital letters F-G labeling the absorption features (e) – (j). Polarization dependence of the Fe K -edge and As K -edge XANES spectra of BaFe_2As_2 . The open red circles in the insets of panels (f) and (i) show the difference spectrum ($\mu(E)_{\phi=45^\circ} - \mu(E)_{\phi=0^\circ}$) with the dashed lines marking some representative energy positions.

it is clear, the anisotropy is strong in the pre-edge (A feature) but persists in all the region of the electronic transitions, peaking again close to the main edge (C feature). The red arrow in the figure calls attention to the fact that the baseline of the spectra coincides in the region below the E_F , excluding a systematic shift of the background signal as a source of the effect. Our analysis will focus on the electronic transitions and in particular in the pre-edge transition.

The significant increase in the pre-edge intensity for a ϕ rotation shows that the mixing between $\text{Fe}3d$ and $\text{As}4p_z$ orbitals form states with a higher density of unoccupied states than the $\text{Fe}3d\text{As}4p_{x,y}$ orbitals. The observed lack of in-plane anisotropy for a χ rotation is expected because the p_x and p_y orbital symmetry is not reduced in a tetragonal environment [45]. Indeed, it is to be noted that the Fe derived $3d$ states are observed via their hybridization with p states and, therefore, the p states symmetries are the relevant properties in discussing the pre-edge polarization dependence. In addition, the very observation of the XAS polarization dependence is unexpected since in itinerant electron systems the ligands are expected to be weak due to screening by conduction electrons. These results add to the importance of the local elec-

tronic properties of itinerant magnets [46].

In Figs.1 (h) – (j), we show the As K -edge spectra data. Here, one can also observe that θ and χ rotations do not change the spectra. Again, the spectra are clearly anisotropic for ϕ rotations, with the absorption edge becoming more intense. This result provides a direct assessment of the As $4p_z$ relative lower electronic filling and larger anisotropic orbital character. We also call attention to the red arrow in 1 (i), showing that the baseline of the spectra coincides in the region below the Fermi level. In the inset, we show the difference spectrum which evidence the large anisotropy of both F and G features.

Our next step is to investigate the composition dependence of the above effects. We start by inspecting the Fe K -edge of Mn and Co substituted samples. Their XANES normalized spectra ($\mu(E)$) are presented in figures 2(a) – (f). The Co substituted sample is a superconductor with $T_{SC} \approx 22$ K whereas the Mn rich sample does not display SC (see Fig. 1(a)). The putative electronic effects of the Co and Mn substitutions would be symmetric with respect to hole and electron doping making these samples ideal for our studies. Concerning θ and χ rotations, the results are similar to what was found

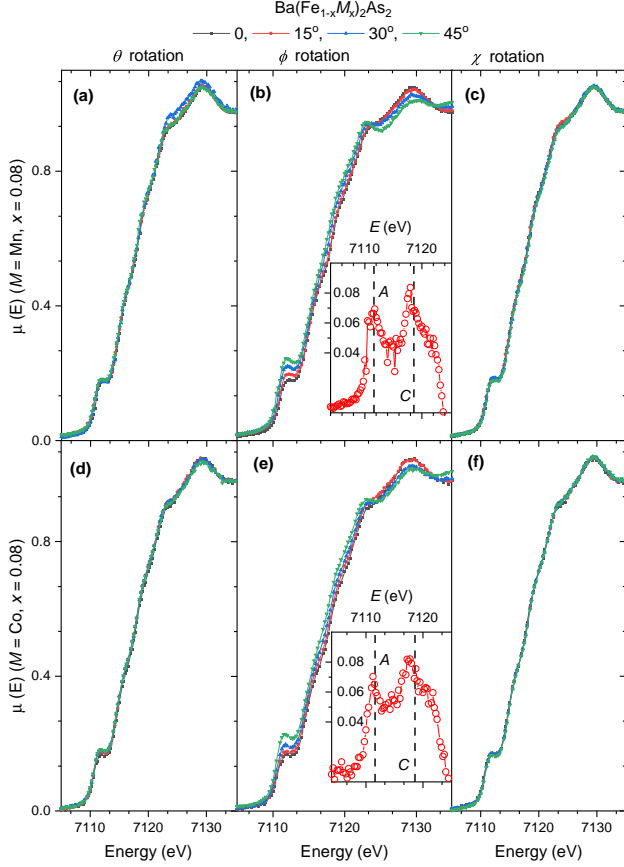


Figure 2. Fe K -edge XANES spectra of (a) – (c) $\text{Ba}(\text{Fe}_{1.92}\text{Mn}_{0.08})_2\text{As}_2$ and (d) – (f) $\text{Ba}(\text{Fe}_{1.92}\text{Co}_{0.08})_2\text{As}_2$ as a function of the polarization (see figures’ top). In all cases, the normalized intensities ($\mu(E)$) are presented. The open red circles in the insets of panels (b) and (e) show the difference spectrum ($\mu(E)_{\phi=45} - \mu(E)_{\phi=0}$) with the dashed lines marking some representative energy positions.

in the parent compound, whereas the data for ϕ rotations suggest a weak composition dependency of this anisotropy.

The insets in figures 2(b) and (e) present the difference spectra for the Mn and Co substituted samples, respectively, and show this effect in more detail. Moreover, the C feature remains markedly anisotropic under ϕ rotations, showing that $\text{Fe}4p_z$ orbitals form bands with a higher unoccupied density of states than the $\text{Fe}4p_{x,y}$ orbitals. This particular result for the BaFe_2As_2 parent compound and doped materials is in contrast to the case of SmFeAsO [28]. In addition, as in previous XANES experiments of iron arsenides, the C feature is not much affected by Co substitution [13, 14, 16, 17] and is here shown to be unaffected by Mn substitution as well.

The composition effect is better observed by our analysis in figures 3(a) – (c). To quantify the intensities anisotropy as a function of ϕ , we fit the Fe K -edge spectra by a Lorentzian (the A_1 peaks) and Gaussian (the A_2 , B , C , D and E peaks) lineshapes plus a Fermi-Dirac function as in figure 3(a). The two peaks in the pre-edge region are clearly present in high-resolution experiments [17] and are suggested by the analy-

sis of our spectra derivatives. Indeed, adopting two peaks is instrumental to extract a consistent fitting analysis. The resonance intensities I_{peak} are estimated from the peak areas, as in the shades of figure 3(a).

The A_1 feature sits just at E_F whereas the B feature lies ≈ 3 eV above it. We thus compare the chemical substitution electronic effects in these two distinct situations by tracking the anisotropy behavior of the A_1 and B features. In figures 3(b) – (c), respectively, we plot the I_{A_1} and I_B normalized intensities as functions of ϕ for the compositions as indicated. Each data set is normalized as $I_{\text{peak}}(\phi)/I_{\text{peak}}(\phi=0)$.

The A_1 peak of the Mn substituted sample is distinctly more anisotropic, but the composition effect is not present in the case of the B feature. Since the latter lies ≈ 3 eV above E_F , it would be hardly affected by chemical substitution, as observed. A naive interpretation about the effect of Mn substitution is that Mn “doping” fills the $\text{Fe}3d\text{As}4p$ hybrid bands with holes, increasing the amount of unoccupied states. At the present “doping” level, however, Mn impurities do not act as charge dopants to BaFe_2As_2 [47, 48] and we shall return to this discussion later by proposing a distinct mechanism for the effects of chemical substitution.

In many instances [30, 31, 49], FEFF calculations provide a first approach to the interpretation of the XANES spectra. In figure 3(d) we show polarization dependent FEFF calculations of the BaFe_2As_2 Fe K -edge spectra, and their derivatives, compared to experimental data. The calculations reproduce well the B – E features position but their polarization dependencies are not fully reproduced. Moreover, the A feature is missed completely, reflecting that FEFF calculations do not capture in full the properties of bound states [30, 31, 49].

If core-hole effects can be considered weak, the nature of the observed transitions can be associated with the element (site) and orbital projected local density of states (LDOS). In figure 3(e), we present the LDOS obtained from FEFF calculations, focusing on the Fe and As derived states. High densities of states are predicted at the positions of the A , B and C features. In particular, the B and C features correlate, respectively, to the LDOS due to the Fe $4s$ and As and Fe $4p$ states. As anticipated in our discussion, the A feature can be associated with a high LDOS derived from Fe $3d$ and As $4p$ states. In addition, our calculations also predict a high density of Fe $4p$ states about this same region, inviting an investigation into the role of the local $\text{Fe}3d4p$ hybridization, which we shall discuss based on quantum chemistry calculations. The inset of figure 3(e), compares the FEFF calculated spectra with and without core-hole effects and the close similarity between the calculations suggests that our discussion is adequate in a first approximation.

We now turn to the As K -edge experiments of other compositions. In figures 4(a) – (f), the normalized intensities ($\mu(E)$) of the As K -edge XANES spectra of the doped samples are presented. Again, the measured spectra are isotropic under θ and χ rotations. In the case of ϕ rotations, however, both $\text{Ba}(\text{Fe}_{1.92}\text{Mn}_{0.08})_2\text{As}_2$ and $\text{Ba}(\text{Fe}_{1.92}\text{Co}_{0.08})_2\text{As}_2$ spectra are polarization-dependent but this time the composition effect is straightforwardly observed by direct inspection of figures 4(b) and 4(e). The insets of the same figures present the

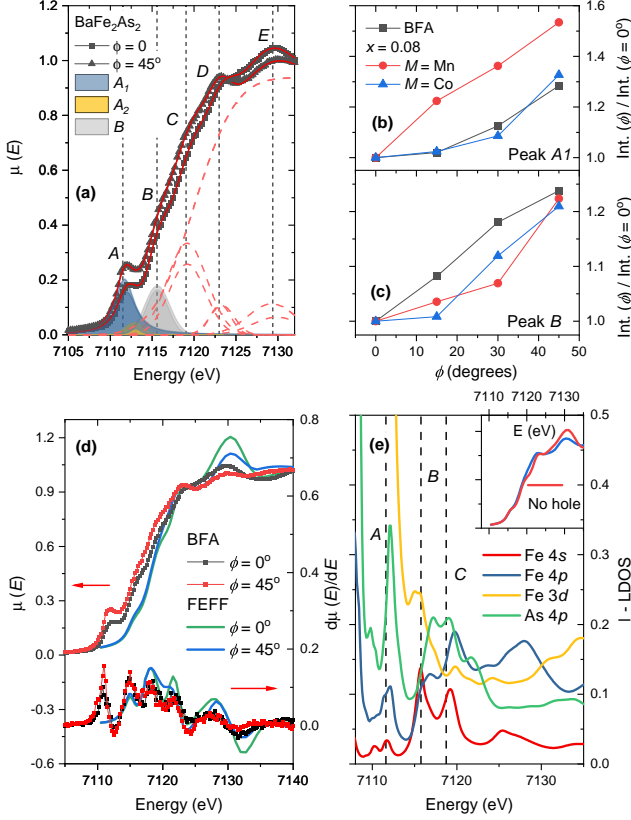


Figure 3. (a) Fe K -edge XANES spectra of BaFe_2As_2 ($\phi = 0$ and $\phi = 45^\circ$) and their respective phenomenological fittings. As shown, two peaks, termed A_1 and A_2 , are included to describe the pre-edge A feature. The shaded regions below the curves are the peak areas which are adopted as the resonance intensities. The obtained intensities are presented in (b) and (c) for, respectively, the A_1 pre-edge peak and the B edge peak as a function of ϕ and composition. In (d) we present polarization-dependent FEFF calculations of the Fe K -edge spectra (left axis) and its derivative (right axis) compared the respective experimental data. A shift of -1.3 eV and a broadening of 1 eV were considered in the calculations. In panel (e), we show the FEFF calculated site and orbital projected LDOS of BaFe_2As_2 . Features A , B and C are presented for comparison to the results. The inset of the figure compares the FEFF calculated spectra ($\phi = 45^\circ$) with and without core-hole effects.

respective difference spectrum ($\mu(E)_{\phi=45} - \mu(E)_{\phi=0}$). The insets are on the same scale, making it clear that the XANES anisotropy is larger for the Mn rich material. Moreover, it is also clear that the edge anisotropy of the Co substituted sample decreases when compared to the case of the parent compound, whereas it increases for the Mn containing sample. Since the As K -edge is a direct probe to the properties of the As $4p_{x,y,z}$ orbitals sitting at about E_F , the distinction between the localization and occupation of the As $4p_z$ orbitals should be more evident, as observed.

The anisotropy of the post edge feature at about 11870 eV, which is about 5 eV above the Fermi level, is also affected by composition, being less intense for the Co substituted sample.

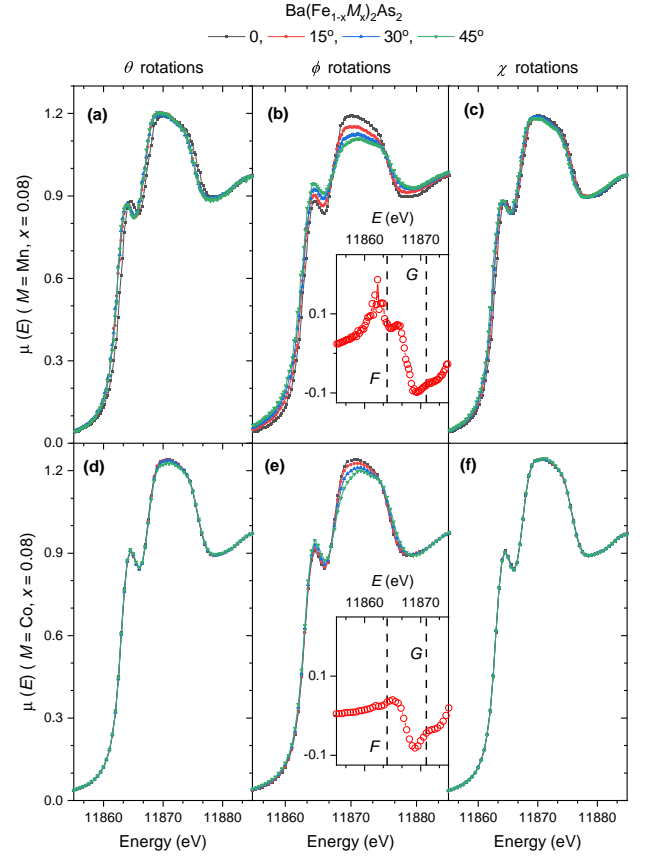


Figure 4. As K -edge XANES spectra of (a) – (c) $\text{Ba}(\text{Fe}_{1.92}\text{Mn}_{0.08})_2\text{As}_2$ and (d) – (f) $\text{Ba}(\text{Fe}_{1.92}\text{Co}_{0.08})_2\text{As}_2$ as a function of the polarization (see figures' top). In all cases, the normalized intensities ($\mu(E)$) are presented. The open red circles in the insets of panels (b) and (e) show the difference spectrum ($\mu(E)_{\phi=45} - \mu(E)_{\phi=0}$) with the dashed lines marking some representative energy positions.

Since this feature is well above the Fermi level, the composition effect is most likely due to the direct effect of the impurity scattering potential [50, 51] and we conclude that Mn impurities act as stronger scattering centers than Co.

To estimate the composition effect in the edge intensity anisotropy as a function of ϕ [$I(\phi)$], we adopt again the integrated areas of the edge features as the approximation to $I(\phi)$. This time, we undertake a direct approach numerically integrating the experimental data, as exemplified in figure 5(a). Indeed, results from a lineshape analysis of the As K -edge are too much dependent on the choice of parameters and we found that a numerical integration suffices to properly capture our results. For each ϕ , $I(\phi)$ is obtained and then the data is normalized as $I(\phi)/I(\phi = 0)$. Results for all samples are shown in figure 5(b). The error bars are estimated by small variations of the integration region. In comparison to the parent compound, the effect of Co substitution is clear, whereas that of Mn is weak but significant.

In Ref. [16], Co substitution is suggested to populate the As derived orbitals. Here, we show that the electrons de-

rived from Co substitution go preferentially to the unoccupied As $4p_z$ states, characterizing a distinct charge transfer anisotropy. By causing an electronic transfer to orbitals along the c -axis, Co substitution unbalances the electron and holes contributions to the transport along this direction, increasing the incoherent scattering in this direction. We thus support the interpretation given in Ref. [52] to the observed BaFe $_2$ As $_2$ inter plane resistivity anisotropy and its increase with Co substitution [52, 53]. Moreover, our results provide a real space picture of the evolving 3D character of the BaFe $_2$ As $_2$ electronic structure as previously probed by angle-resolved photoemission spectroscopy (ARPES) [54].

On the other hand, no change in electronic filling can be invoked as a mechanism to the anisotropy increase caused by Mn substitution. As we will discuss, this effect is connected to the localization of the Fe-derived electronic states. Indeed, isoelectronic substitutions, as observed by resonant inelastic x-ray scattering experiments of Mn- and P-substituted BaFe $_2$ As $_2$ [36, 55], may increase electronic correlations.

We performed polarization-dependent FEFF calculations, aiming at describing two effects: the spectra anisotropy and the composition dependence of this effect. In figure 5(c), we compare the experimental and calculated As K -edges of BaFe $_2$ As $_2$ for $\phi = 0$ and $\phi = 45^\circ$ and their respective derivatives. The overall spectral shape and anisotropy are well reproduced but there is a lack of detail in the effect of the anisotropy. In the calculations, the edge peaks nearly coincide whereas in the experiments the edge intensity of the $\phi = 45^\circ$ spectra sits above the $\phi = 0$ spectra for all compositions.

To simulate the effects of chemical substitution, we performed FEFF calculations replacing one in ten Fe atoms with a dopant (either Mn or Co). This is equivalent to a $x = 0.1$ composition, which is close to our samples for which $x = 0.08$. Three dopant distributions were calculated and then averaged out. In figure 5(d), we compare the difference spectrum ($\mu(E)_{\phi=45} - \mu(E)_{\phi=0}$) obtained from the BaFe $_2$ As $_2$ data (open red circles) and from FEFF calculations of the parent compound and substituted samples (thick lines). As can be observed, the edge polarization dependence is partially reproduced but only a small composition effect is observed in the FEFF calculations.

In figure 5(e), we show the site and orbital projected LDOS obtained from FEFF calculations. The F feature position is marked for comparison. It shows that the main edge is dominated by As $4p$ states, as expected. Moreover, the high density of Fe $3d$ states about the edge position allows the formation of Fe $3d$ As $4p$ hybrid bands making the As K -edge transition sensitive to this mixing. The LDOS of the Fe $4p$ derived states also peaks about the F , as also calculated in the case of the Fe K -edge, further suggesting its relevance to the electronic states about the Fermi energy. Here, due to the As K -edge higher energy, core-hole effects are likely less relevant than for the Fe K -edge, (see inset of figure 3(e)), validating the present discussion in a first approximation.

Whereas our FEFF calculations for the Fe and As K edges are able to support our discussion of the experimental results, it is clear that some aspects of the physics of our system are not captured. This is nothing but an expression of the still un-

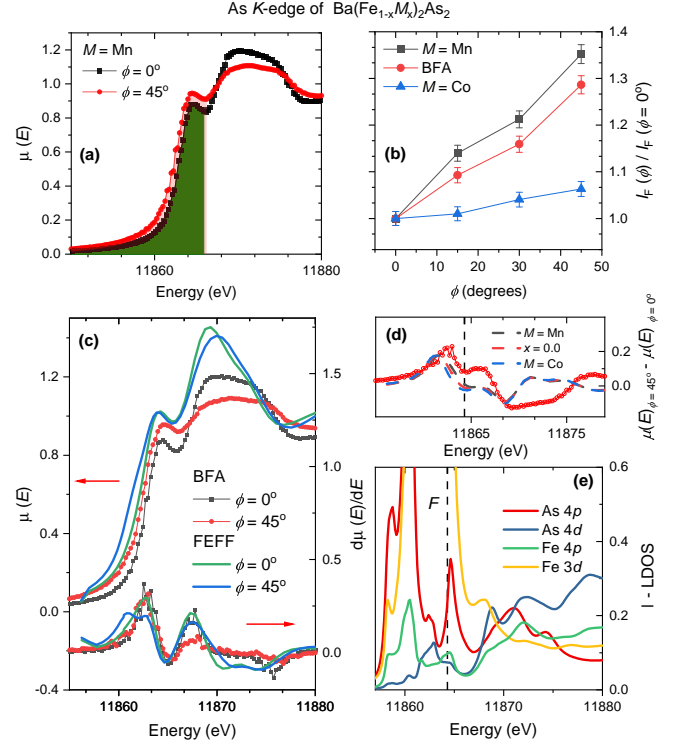


Figure 5. (a) Normalized intensities ($\mu(E)$) of the As K -edge XANES spectra of Ba(Fe $_{1.92}$ Mn $_{0.08}$) $_2$ As $_2$ for $\phi = 0$ and $\phi = 45^\circ$. In each case, the panel shows the spectrum region taken into consideration to perform the numerical integration that represents the F feature intensity ($I_F(\phi)$). (b) The polarization dependence of the F peak intensity as a function of ϕ , for all compositions. In (c) we present polarization-dependent FEFF calculations of the As K -edge spectra (left axis) and its derivative (right axis) compared the respective experimental data. A shift of 1 eV and a broadening of 1.2 eV were considered in the calculations. In panel (d), we present the difference spectrum of the BaFe $_2$ As $_2$ data (open red circles) compared to FEFF calculations of Ba(Fe $_{1-x}$ M $_x$) $_2$ As $_2$, with $M = \text{Mn}$ or Co and $x = 0.1$ (see main text). (e) FEFF calculated site and orbital projected LDOS of BaFe $_2$ As $_2$ focusing on the Fe and As derived electronic states.

resolved character of the electronic states of the FePns materials, that lay in the border between strong and weak electronic correlations. We thus resort to quantum chemistry calculations of the electronic properties of a single FeAs $_4$ distorted tetrahedron, within a multiconfigurational calculation of the orbital states [32, 33, 41, 42].

Being XANES a local probe to electronic structure, it is reasonable to assume that the electronic structure of a single FeAs $_4$ distorted tetrahedron can be connected to the pre-edge feature which, insofar as the Fe K -edge is concerned, is the main focus of our paper. Our results are presented in figure 6 and in table I. In doing that, we are assuming that the XANES transitions in our materials are mainly due to local processes, which excludes the metal-metal charge transfer that is observed in certain transition metal complexes [56, 57]. One can justify this assumption based on the As chemistry, which tends to form complexes with a low bridging character, with

the As 4*p* states well-localized on the As sites. This orbital localization would weaken the Fe-Fe charge transfer that relies on the mediation of the ligand orbitals.

The multiconfigurational calculations results show that the first set of partially occupied states are indeed ligand field (or crystal field) levels formed by hybrid orbitals from Fe3*d* and As4*p* states. In our discussion, we name the $|a_1^*\rangle$, $|b_2^*\rangle$, $|e^*\rangle$ and $|b_1^*\rangle$ molecular orbitals by their Fe 3*d* main character, respectively, d_{z^2} , d_{xy} , d_{xz}/d_{yz} and $d_{x^2-y^2}$. The calculated ligand field splitting of only ≈ 0.3 eV is in qualitative agreement with previous calculations [58].

From table I and from the isosurface plot of the molecular orbital wavefunctions in figure 6, one can observe that all d_{xy} , d_{xz}/d_{yz} and $d_{x^2-y^2}$ hybridize with the As 4*p*_{*x,y,z*} orbitals. The d_{z^2} and d_{xy} orbitals appear in our calculations as nearly degenerate states and are indicated to be virtually double occupied. Electronic transitions are thus dominated by the d_{xz}/d_{yz} and $d_{x^2-y^2}$ hybrid orbitals.

All the d_{xz}/d_{yz} and $d_{x^2-y^2}$ display contributions with p_z orbital character and therefore contribute to the increase of the spectra intensity for ϕ rotations. It should be noted that even if the d_{xy} orbital were not double occupied, it would not contribute to this, since they present no mixing with p_z orbitals. The calculated hybridization pattern of the ligand field orbitals is imposed by the specific properties of the FeAs₄ complex. Indeed, the D_{2d} symmetry would allow the mixing of p_z orbitals into the d_{xy} orbital, whereas it would prevent any p_z orbital mixing with $d_{x^2-y^2}$.

The most prominent feature to be observed from our calculations is the contribution from the Fe4*p* states to ligand field orbitals, forming Fe3*d*4*p* hybrid states. This local *pd* hybridization is acquired by the Fe3*d* states as a formal way of reducing their antibonding character, which is implied by the As⁻³ π -donation. This effect is a mechanism for the localization of the Fe3*d* states, as observed in other coordination complexes [59]. As a consequence, the pre-edge peak in the Fe *K*-edge can be attributed to Fe3*d*4*p* hybridization in Fe complexes [60] and our findings propose that we should reconsider the nature of the pre-edge transition of the Fe *K*-edge of the FePns materials. Indeed, so far in our discussion, as well as in previous works [18, 25–28], the contribution of the Fe4*p* states to the pre-edge was overlooked. We shall argue that this local hybridization is key to understand the effects of Mn substitution.

First, we expect that via the Fe3*d*As4*p* mixing, the Fe *K*-edge results should mirror that of the As *K*-edge, as observed. This expectation, however, does not take into account that the pre-edge intensity may be dominated by transitions to the Fe3*d*4*p* states. This is likely the case of FeSe materials [29], for which the Se *K*-edge clearly indicates that the Se4*p*_{*x,y*} planar orbitals dominate the density of unoccupied states, whereas the contrary is concluded from the Fe *K*-edge.

Mn substitution may weak the Fe3*d*As4*p* mixing, making the Fe orbitals more localized through the mechanisms above explained. In turn, this would make the Fe3*d*4*p*_{*z*} mixing stronger, increasing the observed polarization dependence. In the same direction, the As 4*p* will also become more localized, rendering the As *K* edge spectra more anisotropic.

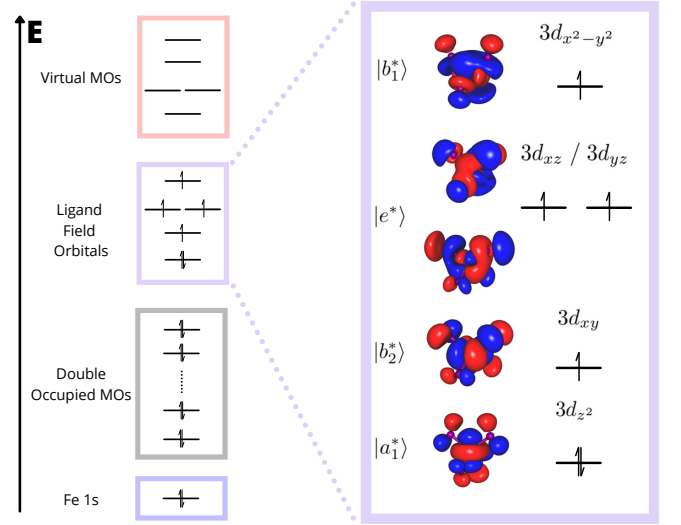


Figure 6. Left panel: the energetic ordering of fully occupied, ligand field and virtual orbitals as obtained from our calculations. Right panel: ligand field molecular orbitals and their ground state configuration based on CAS(6,5)/NEVPT-2/Def2-TZVPP approach [41]. Isosurfaces values are set to 0.006. Our results indicate a ligand field splitting of 0.308 eV. Ligand Orbitals are plotted via the Gabedit program [61]

Both effects are observed in figures 3(b) and 5(b) and we propose that this is the mechanism related to Mn substitution in BaFe₂As₂: Mn impurities localize the Fe3*d* states by changing the Fe3*d*As4*p* mixing. In turn, it shows that hole doping is not the only active mechanism pushing BaFe₂As₂ to a more correlated Mott phase.

IV. SUMMARY AND CONCLUSIONS

We have investigated the polarization dependence of the Fe and As *K*-edges XANES spectra of BaFe₂As₂ and chemically substituted Mn and Co materials of this parent compound. In the case of the Fe *K*-edge, we focused our analysis on the transitions allowed by Fe3*d*As4*p* hybrid orbitals that spam the pre-edge structure of the Fe *K*-edge spectra. In the case of the As *K*-edge, we focused on the edge transitions, probing the As 4*p*_{*x,y,z*} orbitals.

The polarization dependence indicates that Co substitution populates preferentially the hybrid bands with unoccupied states along the *c* axis (p_z orbitals), as concluded from the strong reduction of the As *K*-edge anisotropy. This is a distinct anisotropic charge transfer effect, which may be connected to the transport properties and ARPES experiments of Co doped BaFe₂As₂ [52–54].

Mn substitution, whereas not changing the material electronic filling, increases the anisotropy of the probed electronic states. We attributed this finding to a delicate interplay between the local Fe3*d*4*p* and the metal-ligand Fe3*d*As4*p* mixings, with Mn substitution favoring the Fe3*d* localization by hindering the Fe3*d*As4*p* mixing.

In all cases, the XANES polarization dependence revealed a

Table I. Metal and ligand orbital composition of the FeAs₄ ligand field molecular orbitals. Numbers are given in percentage of normalized wavefunctions. The Final orbital composition analysis was performed adopting the Ros-Schuit partition method via the Multifwn program [62].

Iron orbitals (MO symmetry)		$3d_{z^2}$ (a_1^*)	$3d_{xy}$ (b_2^*)	$3d_{xz}, 3d_{yz}$ (e^*)	$3d_{x^2-y^2}$ (b_1^*)
Ligand Field Relative energies / eV		0.000	0.002	0.260	0.308
Fe orbitals	$4p_z$			4.48	2.25
	$4p_y$ and $4p_x$	5.80		10.32	5.80
As Orbitals	$4p_z$	2.75		2.00	2.38
	$4p_y$ and $4p_x$	0.89	4.15	7.79	5.80

higher density of unoccupied state for orbitals with p_z character, with the results from the Fe K -edge mirroring those of the pnictide K -edge. Our quantum chemistry calculations show this is not the only result that could be expected, since the local Fe $3d4p$ hybridization also contributes to the pre-edge transitions and may dominate its polarization dependence. This is likely the case of FeSe materials [29]. One can thus state a clear distinct behavior of the electronic states of iron arsenides and selenides, with the former presenting a stronger Fe $3d4p$ hybridization, which favors the occupation of orbitals with planar geometry, whereas orbitals along the c -axis remain unoccupied.

Overall, our findings suggest that the interplay between the local Fe $3d4p$ and the metal-ligand Fe $3d$ As(Se) $4p$ mixings is a common thread of the FePns electronic structure, unveiling the key role played by Fe $4p$ states.

V. ACKNOWLEDGMENTS

The authors acknowledge CNPEM-LNLS for the concession of beamtime at the XDS beamline (proposals Nos. 20180194 and 20190123). The XDS beamline staff is acknowledged for their assistance during the experiments. The Fundação de Amparo à Pesquisa do Estado de São Paulo (FAPESP) financial support is acknowledged by M.R.C. (#2019/05150-7 and #2020/13701-0) W.R.S.N. (#2019/23879-4), D.S.C. (#2019/04196-3), J.C.S. (#2018/11364-7 and #2020/12283-0), M.M.P. (#2015/15665-3), P.G.P. and C.A. (#2017/10581-1) and F.A.G. (#2019/25665-1). P.G.P. and C.A. acknowledge the financial support from CNPq: CNPq # 304496/2017-0 and CNPq #310373/2019-0.

-
- [1] Y. Kamihara, T. Watanabe, M. Hirano, and H. Hosono, J. Am. Chem. Soc. **130**, 3296 (2008).
 - [2] H. Hosono and K. Kuroki, Physica C: Superconductivity and its Applications Superconducting Materials: Conventional, Unconventional and Undetermined, **514**, 399 (2015).
 - [3] A. Chubukov, Annual Review of Condensed Matter Physics **3**, 57 (2012).
 - [4] L. de' Medici, G. Giovannetti, and M. Capone, Physical Review Letters **112**, 177001 (2014).
 - [5] Z. P. Yin, K. Haule, and G. Kotliar, Nature Physics **7**, 294 (2011).
 - [6] Z. P. Yin, K. Haule, and G. Kotliar, Nature Materials **10**, 932 (2011).
 - [7] A. S. Sefat, R. Jin, M. A. McGuire, B. C. Sales, D. J. Singh, and D. Mandrus, Physical Review Letters **101**, 117004 (2008).
 - [8] J. S. Kim, S. Khim, H. J. Kim, M. J. Eom, J. M. Law, R. K. Kremer, J. H. Shim, and K. H. Kim, Physical Review B **82**, 024510 (2010).
 - [9] Y. Singh, A. Ellern, and D. C. Johnston, Physical Review B **79**, 094519 (2009).
 - [10] Y. Singh, M. A. Green, Q. Huang, A. Kreyssig, R. J. McQueeney, D. C. Johnston, and A. I. Goldman, Physical Review B **80**, 100403(R) (2009).
 - [11] A. S. Sefat, D. J. Singh, R. Jin, M. A. McGuire, B. C. Sales, and D. Mandrus, Physical Review B **79**, 024512 (2009).
 - [12] V. K. Anand, D. G. Quirinale, Y. Lee, B. N. Harmon, Y. Furukawa, V. V. Ogloblich, A. Huq, D. L. Abernathy, P. W. Stephens, R. J. McQueeney, A. Kreyssig, A. I. Goldman, and D. C. Johnston, Physical Review B **90**, 064517 (2014).
 - [13] E. M. Bittar, C. Adriano, T. M. Garitezi, P. F. S. Rosa, L. Mendonça-Ferreira, F. Garcia, G. d. M. Azevedo, P. G. Pagliuso, and E. Granado, Physical Review Letters **107**, 267402 (2011).
 - [14] V. Balédent, F. Rullier-Albenque, D. Colson, G. Monaco, and J.-P. Rueff, Physical Review B **86**, 235123 (2012).
 - [15] M. Merz, F. Eilers, T. Wolf, P. Nagel, H. van Loehneysen, and S. Schuppler, Physical Review B **86**, 104503 (2012).
 - [16] V. Baledent, F. Rullier-Albenque, D. Colson, J. M. Ablett, and J.-P. Rueff, Physical Review Letters **114**, 177001 (2015).
 - [17] H. Yamaoka, Y. Yamamoto, J.-F. Lin, J. J. Wu, X. Wang, C. Jin, M. Yoshida, S. Onari, S. Ishida, Y. Tsuchiya, N. Takeshita, N. Hiraoka, H. Ishii, K.-D. Tsuei, P. Chow, Y. Xiao, and J. Mizuki, Physical Review B **96**, 085129 (2017).
 - [18] J. Pellicciari, K. Ishii, L. Xing, X. Wang, C. Jin, and T. Schmitt, Applied Physics Letters **118**, 112604 (2021).
 - [19] E. Granado, L. Mendonça-Ferreira, F. Garcia, G. d. M. Azevedo, G. Fabbris, E. M. Bittar, C. Adriano, T. M. Garitezi, P. F. S. Rosa, L. F. Bufaical, M. A. Avila, H. Terashita, and P. G. Pagliuso, Physical Review B **83**, 184508 (2011).
 - [20] J. Cheng, P. Dong, W. Xu, S. Liu, W. Chu, X. Chen, and Z. Wu, Journal of Synchrotron Radiation **22**, 1030 (2015).
 - [21] W. Chu, J. Cheng, S. Chu, T. Hu, A. Marcelli, X. Chen, and Z. Wu, Scientific Reports **3**, 1750 (2013).

- [22] W. Xu, A. Marcelli, B. Joseph, A. Iadecola, W. S. Chu, D. Di Gioacchino, A. Bianconi, Z. Y. Wu, and N. L. Saini, *Journal of Physics-Condensed Matter* **22**, 125701 (2010).
- [23] B. Joseph, A. Ricci, N. Poccia, V. G. Ivanov, A. A. Ivanov, A. P. Menushenkov, N. L. Saini, and A. Bianconi, *Journal of Superconductivity and Novel Magnetism* **29**, 3041 (2016).
- [24] M. Y. Hacisalihoglu, E. Paris, B. Joseph, L. Simonelli, T. J. Sato, T. Mizokawa, and N. L. Saini, *Physical Chemistry Chemical Physics* **18**, 9029 (2016).
- [25] S. Lafuerza, H. Gretarsson, F. Hardy, T. Wolf, C. Meingast, G. Giovannetti, M. Capone, A. S. Sefat, Y.-J. Kim, P. Glatzel, and L. de' Medici, *Physical Review B* **96**, 045133 (2017).
- [26] C. L. Chen, S. M. Rao, C. L. Dong, J. L. Chen, T. W. Huang, B. H. Mok, M. C. Ling, W. C. Wang, C. L. Chang, T. S. Chan, J. F. Lee, J.-H. Guo, and M. K. Wu, *Epl* **93**, 47003 (2011).
- [27] C. L. Chen, C. L. Dong, J. L. Chen, J.-H. Guo, W. L. Yang, C. C. Hsu, K. W. Yeh, T. W. Huang, B. H. Mok, T. S. Chan, J. F. Lee, C. L. Chang, S. M. Rao, and M. K. Wu, *Physical Chemistry Chemical Physics* **13**, 15666 (2011).
- [28] B. C. Chang, Y. B. You, T. J. Shiu, M. F. Tai, H. C. Ku, Y. Y. Hsu, L. Y. Jang, J. F. Lee, Z. Wei, K. Q. Ruan, and X. G. Li, *Physical Review B* **80**, 165108 (2009).
- [29] B. Joseph, A. Iadecola, L. Simonelli, Y. Mizuguchi, Y. Takano, T. Mizokawa, and N. L. Saini, *Journal of Physics: Condensed Matter* **22**, 485702 (2010).
- [30] S. I. Zabinsky, J. J. Rehr, A. Ankudinov, R. C. Albers, and M. J. Eller, *Physical Review B* **52**, 2995 (1995).
- [31] J. J. Rehr and R. C. Albers, *Reviews of Modern Physics* **72**, 621 (2000).
- [32] F. Neese, *WIREs Computational Molecular Science* **2**, 73 (2012).
- [33] F. Neese, *WIREs Computational Molecular Science* **8**, e1327 (2018).
- [34] T. M. Garitezi, C. Adriano, P. F. S. Rosa, E. M. Bittar, L. Bu-faiçal, R. L. d. Almeida, E. Granado, T. Grant, Z. Fisk, M. A. Avila, R. A. Ribeiro, P. L. Kuhns, A. P. Reyes, R. R. Urbano, and P. G. Pagliuso, *Brazilian Journal of Physics* **43**, 223 (2013).
- [35] A. Thaler, H. Hodovanets, M. S. Torikachvili, S. Ran, A. Kracher, W. Straszheim, J. Q. Yan, E. Mun, and P. C. Canfield, *Physical Review B* **84**, 144528 (2011).
- [36] F. A. Garcia, O. Ivashko, D. E. McNally, L. Das, M. M. Piva, C. Adriano, P. G. Pagliuso, J. Chang, T. Schmitt, and C. Monney, *Physical Review B* **99**, 115118 (2019).
- [37] P. F. S. Rosa, C. Adriano, T. M. Garitezi, M. M. Piva, K. Mydeen, T. Grant, Z. Fisk, M. Nicklas, R. R. Urbano, R. M. Fernandes, and P. G. Pagliuso, *Scientific Reports* **4**, 6252 (2014).
- [38] F. A. Lima, M. E. Saleta, R. J. S. Pagliuca, M. A. Eleotério, R. D. Reis, J. Fonseca Júnior, B. Meyer, E. M. Bittar, N. M. Souza-Neto, and E. Granado, *Journal of Synchrotron Radiation* **23**, 1538 (2016).
- [39] B. Ravel and M. Newville, *Journal of Synchrotron Radiation* **12**, 537 (2005).
- [40] L. Hedin and B. I. Lundqvist, *Journal of Physics C: Solid State Physics* **4**, 2064 (1971).
- [41] S. K. Singh, J. Eng, M. Atanasov, and F. Neese, *Coordination Chemistry Reviews Chemical Bonding: "State of the Art"*, **344**, 2 (2017).
- [42] P. Norman and A. Dreuw, *Chemical Reviews* **118**, 7208 (2018).
- [43] F. d. Groot, G. Vankó, and P. Glatzel, *Journal of Physics: Condensed Matter* **21**, 104207 (2009).
- [44] G. Vankó, F. M. F. de Groot, S. Huotari, R. J. Cava, T. Lorenz, and M. Reuther, arXiv:0802.2744 [cond-mat] (2008).
- [45] J. Stöhr and H. C. Siegmann, *Magnetism: From Fundamentals to Nanoscale Dynamics* (Springer-Verlag, Berlin Heidelberg, 2006).
- [46] B. Mounsssef, M. R. Cantarino, E. M. Bittar, T. M. Germano, A. Leithe-Jasper, and F. A. Garcia, *Physical Review B* **99**, 035152 (2019).
- [47] H. Suzuki, T. Yoshida, S. Ideta, G. Shibata, K. Ishigami, T. Kadono, A. Fujimori, M. Hashimoto, D. H. Lu, Z.-X. Shen, K. Ono, E. Sakai, H. Kumigashira, M. Matsuo, and T. Sasagawa, *Physical Review B* **88**, 100501(R) (2013).
- [48] Y. Texier, Y. Laplace, P. Mendels, J. T. Park, G. Friemel, D. L. Sun, D. S. Inosov, C. T. Lin, and J. Bobroff, *EPL (Europhysics Letters)* **99**, 17002 (2012).
- [49] A. L. Ankudinov, B. Ravel, J. J. Rehr, and S. D. Conradson, *Physical Review B* **58**, 7565 (1998).
- [50] T. Kobayashi, M. Nakajima, S. Miyasaka, and S. Tajima, *Physical Review B* **94**, 224516 (2016).
- [51] M. Merz, P. Schweiss, P. Nagel, M.-J. Huang, R. Eder, T. Wolf, H. von Loehneysen, and S. Schuppler, *Journal of the Physical Society of Japan* **85**, 044707 (2016).
- [52] M. Nakajima, M. Nagafuchi, and S. Tajima, *Physical Review B* **97**, 094511 (2018).
- [53] M. A. Tanatar, N. Ni, A. Thaler, S. L. Bud'ko, P. C. Canfield, and R. Prozorov, *Physical Review B* **84**, 014519 (2011).
- [54] S. Thirupathaiah, S. de Jong, R. Ovsyannikov, H. A. Dürr, A. Varykhalov, R. Follath, Y. Huang, R. Huisman, M. S. Golden, Y.-Z. Zhang, H. O. Jeschke, R. Valentí, A. Erb, A. Gloskovskii, and J. Fink, *Physical Review B* **81**, 104512 (2010).
- [55] J. Pelliciari, K. Ishii, Y. Huang, M. Dantz, X. Lu, P. Olalde-Velasco, V. N. Strocov, S. Kasahara, L. Xing, X. Wang, C. Jin, Y. Matsuda, T. Shibauchi, T. Das, and T. Schmitt, *Communications Physics* **2**, 1 (2019).
- [56] C. Gougoussis, M. Calandra, A. Seitsonen, C. Brouder, A. Shukla, and F. Mauri, *Physical Review B* **79**, 045118 (2009).
- [57] D. Cabaret, A. Bordage, A. Juhin, M. Arfaoui, and E. Gaudry, *Physical Chemistry Chemical Physics* **12**, 5619 (2010).
- [58] K. Haule and G. Kotliar, *New Journal of Physics* **11**, 025021 (2009).
- [59] S. Alvarez and J. Cirera, *Angewandte Chemie International Edition* **45**, 3012 (2006).
- [60] R. K. Hocking and E. I. Solomon (Springer, Berlin, Heidelberg, 2012) pp. 155–184.
- [61] A.-R. Allouche, *Journal of Computational Chemistry* **32**, 174 (2011).
- [62] T. Lu and F. Chen, *Journal of Computational Chemistry* **33**, 580 (2012).